True Gravity in Ocean Circulation

Peter C Chu[1]

[1]Naval Postgraduate School

November 22, 2022

Abstract

Two related issues in oceanography are addressed: (1) the unit vector (k) normal to the Earth spherical/ellipsoidal surface is not vertical (called deflected-vertical) since the vertical is in the direction of the true gravity, g = iγ_λ+jγ_φ+kg_z, with (λ, φ, z) the (longitude, latitude, depth) and (i, j, k) the corresponding unit vectors; and (2) the true gravity g is replaced by the standard gravity (-g$_0$k, g$_0$ = 9.81 m/s^2). In the spherical/ellipsoidal coordinate (λ, φ, z) and local coordinate (x, y, z), the z-direction is along k (positive upward). The spherical/ellipsoidal surface and (x, y) plane are perpendicular to k, and therefore they are not horizontal (called deflected-horizontal) since the horizontal surfaces are perpendicular to the true gravity g such as the geoid surface. In the vertical-deflected coordinates, the true gravity g has deflected-horizontal component, g$_h$ = iγ_λ+jγ_φ (or = ig_x+jg_y), which is neglected completely in oceanography. This study uses the classic ocean circulation theories to illustrate the importance of g$_h$ in the vertical-deflected coordinates. The standard gravity (-g$_0$k) is replaced by the true gravity g in the existing equations for geostrophic current, thermal wind relation, and Sverdrup-Stommel-Munk wind driven circulation to obtain updated formulas. The proposed non-dimensional (C, D, F) numbers are calculated from four publicly available datasets to prove that g$_h$ cannot be neglected against the Coriolis force, density gradient forcing, and wind stress curl.

True Gravity in Ocean Circulation

Peter C. Chu

Department of Oceanography, Naval Postgraduate School, Monterey, CA, USA.

Corresponding author: Peter Chu (pcchu@nps.edu)

Key Points:

- Normal to Earth spherical/ellipsoidal surface is not vertical. True gravity **g** represents vertical with longitudinal-latitudinal components
- Replacement of the standard gravity $-g_0\mathbf{k}$ (g_0=9.81 m s^{-2}) by $\mathbf{g}(\lambda, \varphi, z)$ in oceanography leads to new physics
- With four publicly available datasets, the longitudinal and latitudinal components of the true gravity are proved non-negligible

Abstract

Two related issues in oceanography are addressed: (1) the unit vector (**k**) normal to the Earth spherical/ellipsoidal surface is not vertical (called deflected-vertical) since the vertical is in the direction of the true gravity, $\mathbf{g} = \mathbf{i}g_\lambda+\mathbf{j}g_\varphi+\mathbf{k}g_z$, with ($\lambda$, φ, z) the (longitude, latitude, depth) and (**i**, **j**, **k**) the corresponding unit vectors; and (2) the true gravity **g** is replaced by the standard gravity ($-g_0\mathbf{k}$, $g_0 = 9.81$ m/s^2). In the spherical/ellipsoidal coordinate (λ, φ, z) and local coordinate (x, y, z), the z-direction is along **k** (positive upward). The spherical/ellipsoidal surface and (x, y) plane are perpendicular to **k**, and therefore they are not horizontal (called deflected-horizontal) since the horizontal surfaces are perpendicular to the true gravity **g** such as the geoid surface. In the vertical-deflected coordinates, the true gravity **g** has deflected-horizontal component, $\mathbf{g}_h = \mathbf{i}g_\lambda+\mathbf{j}g_\varphi$ (or $= \mathbf{i}g_x+\mathbf{j}g_y$), which is neglected completely in oceanography. This study uses the classic ocean circulation theories to illustrate the importance of $\mathbf{g}_h$ in the vertical-deflected coordinates. The standard gravity ($-g_0\mathbf{k}$) is replaced by the true gravity **g** in the existing equations for geostrophic current, thermal wind relation, and Sverdrup-Stommel-Munk wind driven circulation to obtain updated formulas. The proposed non-dimensional (C, D, F) numbers are calculated from four publicly available datasets to prove that $\mathbf{g}_h$ cannot be neglected against the Coriolis force, density gradient forcing, and wind stress curl.

Plain Language Summary

Oceanographers use the spherical/ellipsoidal coordinates (λ, φ, z) to represent (longitude, latitude, depth) and local coordinates (x, y, z) to represent (eastward, northward, depth) with (**i**, **j**, **k**) the corresponding unit vectors. Here, **k** is normal to the Earth spherical/ellipsoidal surface but not in the vertical since the vertical is in the direction of the true gravity, $\mathbf{g} = \mathbf{i}g_\lambda+\mathbf{j}g_\varphi+\mathbf{k}g_z$. The z-direction is called the deflected-vertical. Correspondingly, the spherical/ellipsoidal surface and (x, y) plane are perpendicular to **k**, and therefore they are not horizontal (called deflected-horizontal) since the horizontal surfaces are perpendicular to the true gravity **g** such as the geoid surface. In the vertical-deflected (λ, φ, z) and (x, y, z) coordinates, the true gravity **g** has deflected-horizontal component $\mathbf{g}_h = \mathbf{i}g_\lambda+\mathbf{j}g_\varphi$ (or $= \mathbf{i}g_x+\mathbf{j}g_y$), which is neglected completely in oceanography. This study uses four publicly available datasets and classical ocean circulation theory to prove that $\mathbf{g}_h$ cannot be neglected in oceanography.

1 Introduction

Oceanographers use the Earth-fixed coordinate system with (λ, φ, z) representing the longitude, latitude, and spherical normal (or depth) with (**i**, **j**, **k**) the corresponding unit vectors. The unit vector **k** is normal to the Earth spherical surface (polar spherical coordinate) or to the ellipsoidal surface (ellipsoidal coordinate), and does not represent the true vertical direction since the Earth true gravity **g** ($= g_\lambda\mathbf{i} + g_\varphi\mathbf{j} + g_z\mathbf{k}$) represents the true vertical direction. We may call the direction of **k** the deflected-vertical or z-direction. The angle between -**k** and **g** is the vertical deflection. The spherical (or ellipsoidal) surfaces are not the horizontal surfaces since the equipotential surfaces of **g** such as the geoid surface represent the horizontal surfaces. Figure 1 shows the global static geoid height (N) varying from -106.20 m (minimum) to 85.83 m (maximum) from the EIGEN-6C4 model (Förste et al., 2014; Ince et al., 2019), which was developed jointly by the GFZ Potsdam and GRGS Toulouse up to degree and order 2190. The geoid surface ($z = N$) is the **true horizontal surface**, which is obviously different from the Earth spherical/ellipsoidal surface ($z = 0$).

The two (λ, φ, z) coordinate systems (spherical and ellipsoidal) are called the vertical-deflected coordinates. Appendix A describes the difference between them. In addition to the (λ, φ, z) coordinates, oceanographers also use the local coordinate (x, y, z),

$$\frac{\partial}{\partial x} = \frac{1}{R\cos\varphi}\frac{\partial}{\partial \lambda}, \quad \frac{\partial}{\partial y} = \frac{1}{R}\frac{\partial}{\partial \varphi} \tag{1}$$

where the (x, y) plane is perpendicular to $\mathbf{k}$, and therefore is not the true horizontal plane. Thus, the local coordinate is also classified as the vertical-deflected coordinate system.

In addition to the use of vertical-deflected coordinate system, oceanographers simplify the true gravity vector $\mathbf{g}$ into the standard gravity $-g_0\mathbf{k}$ (g_0 = 9.81 m s^{-2}). The longitudinal-latitudinal component of the true gravity, $\mathbf{g}_h$ ($= g_\lambda\mathbf{i} + g_\varphi\mathbf{j}$) is totally neglected. Use of the standard gravity ($-g_0\mathbf{k}$) instead of the true gravity $\mathbf{g}$ is based on the comparison that the strength of the z-component $|g_z|$ is 5-6 orders of magnitude larger than the strength of its longitudinal-latitudinal component $|\mathbf{g}_h|$. Recent study (Chu, 2021) shows such simplification may not be correct. Because such a huge difference in magnitude between the components in $\mathbf{k}$ and in ($\mathbf{i}$, $\mathbf{j}$) also occurs in the pressure gradient force. But, the pressure gradient force in ($\mathbf{i}$, $\mathbf{j}$) is never neglected against the pressure gradient force in $\mathbf{k}$. Thus, the feasibility of using the standard gravity ($-g_0\mathbf{k}$) in oceanography needs to be investigated. Updated ocean dynamic equations including $\mathbf{g}_h$ were proposed (Chu, 2021).

The objective of this paper is to report the follow-up work showing the importance of $\mathbf{g}_h$ in ocean circulation such as the geostrophic current, thermal wind, wind-driven circulation such as the Sverdrup and Stommel volume transports by the comparison between $\mathbf{g}_h$ and other forcing terms such as the density gradient, Coriolis force, and surface wind stress with corresponding non-dimensional (C, D, F) numbers.

The rest of the paper is outlined as follows. Section 2 describes the vertical-true coordinate versus vertical-deflected coordinate. Section 3 presents the dynamic equation with the true gravity. Section 4 describes the data sources. Sections 5-7 show the geostrophic current, thermal wind, and wind-driven circulation with $\mathbf{g}_h$. Section 8 presents the conclusions. Appendices A-D present the two vertical-deflected coordinate systems and the basic information about the true gravity $\mathbf{g}$ and related disturbing static gravity potential T. Appendix E presents the derivation of the combined Sverdup-Stommel-Munk equation with $\mathbf{g}_h$.

2 Vertical-True Coordinate versus Vertical-Deflected Coordinate

The true vertical direction $\mathbf{e}_3$ is with the true gravity $\mathbf{g}$,

$$\mathbf{g}(\lambda,\varphi,z) = |\mathbf{g}(\lambda,\varphi,z)|\mathbf{e}_3(\lambda,\varphi,z)\ . \tag{2}$$

The true horizonal surfaces are the equipotential surfaces of the true gravity [$V(\lambda,\varphi,z)$] (see Appendix C). The geoid is one of them (see Figure 1). On a true horizontal surface, the orthogonal unit vectors are represented by [$\mathbf{e}_1(\lambda,\varphi,z)$, $\mathbf{e}_2(\lambda,\varphi,z)$], but not ($\mathbf{i}$, $\mathbf{j}$). The coordinate system represented by ($\mathbf{e}_1$, $\mathbf{e}_2$, $\mathbf{e}_3$) is called the vertical-true coordinate system. In the vertical-true coordinate, the true gravity $\mathbf{g}$ has the true-vertical component only and no true-horizontal component.

However, it is not feasible to use the ($\mathbf{e}_1$, $\mathbf{e}_2$, $\mathbf{e}_3$) coordinate since the unit vectors [$\mathbf{e}_1(\lambda,\varphi,z)$, $\mathbf{e}_2(\lambda,\varphi,z)$, $\mathbf{e}_3(\lambda,\varphi,z)$] vary at each point inside the oceans, and it is almost impossible to convert any ocean model (theoretical or numerical) with the standard gravity ($-g_0\mathbf{k}$) into the model with the true gravity **g** using the reference coordinates with the unit vectors [$\mathbf{e}_1(\lambda,\varphi,z)$, $\mathbf{e}_2(\lambda,\varphi,z)$, $\mathbf{e}_3(\lambda,\varphi,z)$]. Besides, all the existing ocean models and datasets are represented in the vertical-deflected coordinate system [(λ, φ, z) or (x, y, z)]. Also, even in the geodetic community, the gravity models are represented in the vertical-deflected coordinate (λ, φ, z). Thus, the feasible approach in oceanography is to keep the traditional vertical-deflected coordinates, and to replace the standard gravity ($-g_0\mathbf{k}$) by the true gravity **g** ($= \mathbf{g}_h - g_0\mathbf{k}$) in dynamic equations.

3 Dynamic Equation with the True Gravity

Application of the Newton's second law of motion into the oceans with the Boussinesq approximation (replacement of density ρ by a constant ρ_0 except ρ being multiplied by the gravity and incompressibility) is given by (Chu, 2021)

$$\rho_0\left[\frac{D\mathbf{U}_3}{Dt}+2\mathbf{\Omega}\times\mathbf{U}\right]=-\nabla_3 p+\mathbf{g}+\rho_0(\mathbf{F}_h+\mathbf{F}_v) \tag{3a}$$

$$\nabla\bullet\mathbf{U}+\frac{\partial w}{\partial z}=0 \tag{3b}$$

if the pressure gradient force, true gravity **g** (see Appendices B and C), and friction are the only real forces. Here, $\nabla_3\equiv\mathbf{i}\frac{1}{R\cos\varphi}\frac{\partial}{\partial\lambda}+\mathbf{j}\frac{1}{R}\frac{\partial}{\partial\varphi}+\mathbf{k}\frac{\partial}{\partial z}$, and $\nabla\equiv\mathbf{i}\frac{1}{R\cos\varphi}\frac{\partial}{\partial\lambda}+\mathbf{j}\frac{1}{R}\frac{\partial}{\partial\varphi}$ are the 3D and 2D vector differential operators in the polar spherical coordinates; $\mathbf{\Omega}=\Omega\left(\mathbf{j}\cos\varphi+\mathbf{k}\sin\varphi\right)$, is the Earth rotation vector with $\Omega = 2\pi/(86164\ \text{s})$ the Earth rotation rate; ρ is the density; ρ_0 = 1,028 kg/m^3, is the characteristic density; **U** = (u, v), is the 2D longitudinal-latitudinal velocity vector; w is the z-component velocity; $\mathbf{U}_3$ =(**U**, w), is the 3D velocity vector; p is the pressure; D/Dt is the total time rate of change; ($\mathbf{F}_h$, $\mathbf{F}_v$) are the frictional forces with longitudinal-latitudinal and z-directional shears represented by

$$\mathbf{F}_h = A\nabla^2\mathbf{U},\quad \mathbf{F}_v=\frac{\partial}{\partial z}\left(K\frac{\partial\mathbf{U}}{\partial z}\right) \tag{4}$$

where (A, K) are the corresponding eddy viscosities. The true gravity **g** is represented by [see Eq.(D5) in Appendix D]

$$\mathbf{g}(\lambda,\varphi,z)\approx\mathbf{g}_h-g_0\mathbf{k}\approx g_0\nabla N(\lambda,\varphi)-g_0\mathbf{k} \tag{5}$$

for oceanography. Substitution of (5) into (3a) leads to the equation in the longitudinal and latitudinal directions,

$$\rho_0\left[\frac{D\mathbf{U}}{Dt}+2\mathbf{\Omega}\times\mathbf{U}\right]=-\nabla p+\rho\mathbf{g}_h+\rho_0(\mathbf{F}_h+\mathbf{F}_v) \tag{6}$$

and the equation in the z-direction (hydrostatic balance),

$$\frac{\partial p}{\partial z}=-\rho g_0 \tag{7}$$

4 Data Sources

Four datasets were used in this study: (a) the global static gravity model EIGEN-6C4 (http://icgem.gfz-potsdam.de/home), which was developed jointly by the GFZ Potsdam and GRGS Toulouse up to degree and order 2190, for the geoid height $N(\lambda, \varphi)$, (b) the climatological annual mean hydrographic data from the NOAA/NCEI World Ocean Atlas 2018 (WOA18) (https://www.nodc.noaa.gov/OC5/woa18/) for the sea water density $\rho(\lambda, \varphi, z)$, (c) the climatological annual mean surface wind stress ($\tau_\lambda, \tau_\varphi$) from the Surface Marine Data (SMD94) (http://iridl.ldeo.columbia.edu/SOURCES/.DASILVA/.SMD94/.climatology/) (da Silva et al., 1994), and (d) the Ocean Surface Current Analysis Real-time (OSCAR) third degree resolution 5-day mean surface current vectors (https://podaac-tools.jpl.nasa.gov/drive/files/allData/oscar/) $\mathbf{U}(\lambda, \varphi)$. The OSCAR data represent averaged surface currents in the z-direction over the top 30 m of the upper ocean, which consist of a geostrophic component with a thermal wind adjustment using satellite sea surface height, and temperature and a wind-driven ageostrophic component using satellite surface winds (https://doi.org/10.5067/OSCAR-03D01).

5 Geostrophic Current

For steady-state low Rossby number (negligible nonlinear advection) flow without friction (i.e., $D\mathbf{U}/Dt = 0$, $\mathbf{F}_h = 0$, $\mathbf{F}_v = 0$), Eq.(6) is simplified into

$$2\mathbf{\Omega} \times \mathbf{U} = -\frac{1}{\rho_0}\nabla p + \frac{\rho}{\rho_0} g_0 \nabla N \quad (8)$$

where (5) is used. Here, Eq.(8) includes the effect of $\mathbf{g}_h$ on the geostrophic motion, and can be rewritten as

$$\boxed{f\rho_0 \mathbf{U} = \mathbf{k} \times (\nabla p - \rho g_0 \nabla N)} \quad (9)$$

A non-dimensional C-number is defined by (Chu 2021)

$$C(\lambda,\varphi) = \frac{|\mathbf{g}_h|}{|f||\mathbf{U}|} = \frac{g_0 |\nabla N(\lambda,\varphi)|}{|f||\mathbf{U}(\lambda,\varphi)|} \quad (10)$$

to identify the relative importance of $\mathbf{g}_h$ versus the Coriolis force. Chu (2021) calculated the C-number at $z = 0$ from the geoid (N) data from the EIGEN-6C4 gravity model and the surface current data $\mathbf{U}(\lambda, \varphi)$ data from the OSCAR third degree resolution 5-day mean surface current vectors on 26 February 2020, and showed that $\mathbf{g}_h$ cannot be neglected against the Coriolis force due to large values of the C-number.

On the Earth spherical surface ($z = 0$),

$$p|_{z=0} = \rho g_0 S, \quad \rho|_{z=0} \cong \rho_0 \quad (11)$$

where S is the sea surface height. Substitution of (11) into (9) leads to

$$\boxed{\mathbf{U}|_{z=0} = \frac{g_0}{f}\mathbf{k} \times \nabla D, \quad D = S - N} \quad (12)$$

where D is the dynamic ocean topography.

6 Thermal Wind Relation

Differentiation of Eq.(9) with respect to z and use of Eq.(7) lead to the thermal wind relation,

$$\boxed{f\frac{\partial \mathbf{U}}{\partial z} = \mathbf{k} \times \left[-(g_0/\rho_0)\nabla \rho + \Theta^2 \nabla N\right], \quad \Theta^2 \equiv -\left(\frac{g_0}{\rho_0}\frac{\partial \rho}{\partial z}\right)} \quad (13)$$

where Θ is the buoyancy frequency. The second term in the righthand side represents the effect of $\mathbf{g}_h$. The WOA18 annual mean temperature and salinity data with (1°×1°) horizontal resolution and 102 vertical levels (0 to 5500 m depth) were used to compute the density ρ. With the given density (ρ) and marine geoid height (N), two vectors in the thermal wind relation (13), $(g_0/\rho_0)\nabla\rho$ (representing deflected-horizontal density gradient) and $\Theta^2 \nabla N$ (representing $\mathbf{g}_h$)

were computed at all grid points for all the vertical levels (z = 0 to -5,500 m). The vector $(g_0/\rho_0)\nabla\rho$ at the four levels, z = 0, -500 m, -1,000 m, and -2,000 m, are presented with the vector plots (Figure 2a), contour plots of the magnitudes $|(g_0/\rho_0)\nabla\rho|$ (Figure 2b), and histograms (Figure 2c) of $|(g_0/\rho_0)\nabla\rho|$. The magnitude $|(g_0/\rho_0)\nabla\rho|$ has the mean of 13.45 Eotvos (1 Eotvos = $10^{-9}s^{-2}$) at the surface (z = 0), 2.154 Eotvos at z = -500 m, 1.245 Eotvos at z = -1,000 m, and 0.5615 Eotvos at z = - 2,000 m.

Besides, the square of the annual mean buoyancy frequency Θ^2 was also computed at each grid point from the density using Eq.(13). With the global N and Θ^2 data, the vectors of $-\Theta^2\nabla N$ (geostrophic shear due to the horizontal gravity component) on the four levels, z = 0, -500 m, -1,000 m, and -2,000 m, with the vector plots in Figure 3a and contour plots of the magnitudes $|\Theta^2\nabla N|$ in Figure 3b. The histograms (Figure 3c) of $|\Theta^2\nabla N|$ show the mean of 1.128 Eotvos at z = 0, 0.4789 Eotvos at z = -500 m, 0.4389 Eotvos at z = -1,000 m, and 0.3894 Eotvos at z = -2,000 m.

The importance of $\mathbf{g}_h$ can also be identified by a non-dimensional D number

$$D = \frac{O\left(\left|\Theta^2\nabla N\right|\right)}{O\left(\left|(g_0/\rho_0)\nabla\rho\right|\right)} \tag{14}$$

Taking the calculated mean values of $|(g_0/\rho_0)\nabla\rho|$ and $|\Theta^2\nabla N|$ for each z-level as the characteristic scales, the D-number was calculated for each z-level (Figure 4). The D-number increases with depth almost monotonically from a small value (0.084) at z = 0, 0.222 at z = -500 m, 0.353 at z = -1,000 m, 0.693 at z = -2,000 m, 0.814 at z = -3,000 m, 1.087 at z = -4,000 m, and 1.576 at z = -5,000 m.

7 Wind Driven Circulation

7.1 Combined Sverdrup-Stommel-Munk Equation

For steady-state low Rossby number (negligible nonlinear advection) flow with friction (i.e., D**U**/Dt = 0, and $\mathbf{F}_h \neq 0$, $\mathbf{F}_v \neq 0$), Eq.(6) is simplified into

$$\rho_0\left(2\mathbf{\Omega}\times\mathbf{U}\right) = -\nabla p + \rho\mathbf{g}_h + \rho_0(\mathbf{F}_h + \mathbf{F}_v)\,. \tag{15}$$

With the wind stress (τ_x, τ_y) as the forcing at the rigid-lid ocean surface (z = 0) and negligible bottom stress (Sverdrup 1947, Munk 1950) or taking the Rayleigh friction as the bottom stress (Stommel 1948) at the flat bottom (z = -H), a combined Sverdrup-Stommel-Munk equation in the local coordinate system (1) as the tradition is derived from (15) (see derivation in Appendix E)

$$\boxed{-A\nabla^4\Psi + \gamma\nabla^2\Psi + \beta\frac{\partial\Psi}{\partial x} = \frac{1}{\rho_0}\left[\operatorname{curl}\boldsymbol{\tau} + g_0\int_{-H}^{0} J(\rho, N)dz\right]} \tag{16}$$

where β = (2Ωcosφ)/R; $J(\rho,N) \equiv [(\partial\rho/\partial x)(\partial N/\partial y) - (\partial\rho/\partial y)(\partial N/\partial x)]$, is the Jacobian of ρ and N; and Ψ is the volume transport stream function defined by

$$\frac{\partial\Psi}{\partial x} = \int_{-H}^{0} vdz, \quad \frac{\partial\Psi}{\partial y} = -\int_{-H}^{0} udz \tag{17}$$

After changing the flat bottom into non-flat bottom topography, $z = -H(x, y)$, Eq.(17) becomes,

$$-A\nabla^4\Psi + \gamma\nabla^2\Psi + \beta\frac{\partial\Psi}{\partial x} = \frac{1}{\rho_0}\left[\text{curl}\,\boldsymbol{\tau} + g_0\int_{-H(x,y)}^{0} J(\rho, N)dz\right] + \begin{matrix}\text{Bottom Topographic}\\ \text{Effect Term}\end{matrix} \tag{18}$$

Here, the bottom topographic effect on the volume transport is beyond the scope of this study, and therefore is not identified. The second term in the righthand side is an additional term called "Joint Effect of Baroclinicity and true Gravity" (JEBAG)

$$\text{JEBAG} = g_0\int_{-H(x,y)}^{0}\left(\frac{\partial\rho}{\partial x}\frac{\partial N}{\partial y} - \frac{\partial\rho}{\partial y}\frac{\partial N}{\partial x}\right)dz \tag{19}$$

7.2. Global Surface Wind Stress Curl and JEBAG

The relative importance of wind stress curl and JEBAG on the volume transport streamfunction Ψ is identified using the EIGEN-6C4 geoid data for the geoid $N(x, y)$, SMD94 annual mean surface wind stress (τ_x, τ_y) data for computing the surface wind stress curl, and WOA18 annual mean hydrographic data for computing the sea water density $\rho(x, y, z)$. The calculated global surface wind stress curl (Figure 5) and JEBAG (simplified as 'J' in Figure 6) have comparable magnitudes with different horizontal distributions (Figure 5a and Figure 6a). The histograms of (curl $\boldsymbol{\tau}$) (Figure 5b) and JEBAG (Figure 6b) show nearly symmetric with mean values near zero. The histograms of the absolute values, |curl $\boldsymbol{\tau}$| (Figure 5c) and |JEBAG| (Figure 6c) show near Gamma distribution with the shape parameter of 1 and scale parameter of 2. |JEBAG| has comparable mean and standard deviation (3.448, 4.283)$\times10^{-8}$ Nm^{-3}, with |curl $\boldsymbol{\tau}$| (4.984, 4.052)$\times10^{-8}$Nm^{-3}; but has two-time larger skewness and kurtosis (2.19, 8.12), than |curl $\boldsymbol{\tau}$| (1.081, 4.137). The statistics show comparable forcing of JEBAG and (curl $\boldsymbol{\tau}$) in the ocean circulation.

Note that large |JEBAG| values occurring around the Gulf Stream and Antarctic Circumpolar Circulation regions. The reason is explained as follows. From Eq.(16) the JEBAG can be rewritten by

$$\text{JEBAG} = \mathbf{k}\bullet\left(\mathbf{B}\times\mathbf{g}_h\right) = |\mathbf{B}||\mathbf{g}_h|\sin\alpha, \quad \mathbf{B} \equiv \int_{-H}^{0}\nabla\rho dz, \quad \mathbf{g}_h = g_0\nabla N \tag{20}$$

where the vector $\mathbf{B}$ represents the baroclinicity; and α is the angle between $\mathbf{B}$ and $\mathbf{g}_h$. The |JEBAG| value depends on the angle α and the intensities of the two vectors |$\mathbf{B}$| and |$\mathbf{g}_h$|. Near the Gulf Stream and Antarctic Circumpolar Circulation regions, the vector $\mathbf{B}$ is in the north-south direction usually with large magnitude. However, the vector $\mathbf{g}_h$ is in the east-west direction (Figure 1) with noticeable magnitude (i.e., ∇N). Near 90° cross angle α may be the major reason to cause large |JEBAG| values there.

Importance of $\mathbf{g}_h$ can be identified by a non-dimensional F number from the ratio between the JEBAG versus the surface wind stress curl,

$$F(\lambda,\varphi) = \frac{|\text{JEBAG}(\lambda,\varphi)|}{|\text{curl}\,\boldsymbol{\tau}(\lambda,\varphi)|} \tag{21}$$

The comparable forcing between $\mathbf{g}_h$ and surface wind stress curl is also shown in the world ocean distribution of F values (Figure 7a). The histogram of F (Figure 7b) indicates a positively skewed distribution with a long tail extending to values larger than 10. The statistical characteristics of F are 1.053 as the mean, 1.647 as the standard deviation, 2.779 as the skewness, and 11.36 as the kurtosis. The statistics show that $\mathbf{g}_h$ cannot be neglected in comparison to the surface wind stress curl in the wind-driven circulation.

7.3. Sverdrup and Stommel Volume Transports

The Sverdrup equation is obtained by setting $A = 0$ (no deflected-horizontal eddy viscosity), and $\gamma = 0$ (no bottom friction) in (18)

$$\beta \frac{\partial \Psi}{\partial x} = \frac{1}{\rho_0}\left[\text{curl}\, \boldsymbol{\tau} + g_0 \int_{-H(x,y)}^{0} J(\rho, N) dz \right] \tag{22}$$

The Stommel equation is obtained by setting $A = 0$ (no deflected-horizontal eddy viscosity) in (18),

$$\gamma \nabla^2 \Psi + \beta \frac{\partial \Psi}{\partial x} = \frac{1}{\rho_0}\left[\text{curl}\, \boldsymbol{\tau} + g_0 \int_{-H}^{0} J(\rho, N) dz \right], \quad \gamma = 10^{-6} \tag{23}$$

The standard boundary conditions are used: $\Psi = 0$ at the eastern boundary for the Sverdrup equation , and at all boundaries for the Stommel equation. In the Southern Ocean, the cyclic boundary condition is used at 20°E section across the Africa and Antarctic continents. Three numerical integrations are conducted to solve Eqs(22) and (23): (a) Ψ_1 with both (curl $\boldsymbol{\tau}$) and JEBAG, (b) Ψ_2 with (curl $\boldsymbol{\tau}$) only, and (c) Ψ_3 with JEBAG only for the Sverdrup (Figure 8) and Stommel (Figure 9) volume transport streamfunctions. Relative root mean differences between (Ψ_1, Ψ_2) and (Ψ_1, Ψ_3) for both equations,

$$\text{RRMSD}(\Psi_1, \Psi_n) = \frac{\sqrt{\sum_i \sum_j \left[\Psi_1(i,j) - \Psi_n(i,j) \right]^2}}{\sqrt{\sum_i \sum_j \left[\Psi_1(i,j) \right]^2}}, \quad n = 2, 3 \tag{24}$$

are calculated with using the true gravity (Ψ_1) taken as the reference. RRMSD between Ψ_1 (winds and JEBAG) (Figures 8a and 9a), Ψ_2 (winds only) (Figure 8b and 9b) is 0.373 for the Sverdrup volume transport streamfunction, and 0.405 for the Stommel volume transport stream function. RRMSD between Ψ_1 (winds and JEBAG) and Ψ_3 (JEBAG only) (Figures 8c and 9c) is 0.767 for the Sverdrup volume transport streamfunction, and 0.848 for the Stommel volume transport streamfunction.

7.4 Comparison with observations

Strong Sverdrup (Figure 8) and Stommel (Figure 9) volume transports are identified associated with the Antarctic Circumpolar Current (ACC). The Sverdrup volume transport is 78 Sv with wind stress curl and JEBAG (Figure 8a) and 37 Sv with wind stress curl only (Figure 8b). The Stommel volume transport is 50 Sv with wind stress curl and JEBAG (Figure 9a) and 28 Sv with wind stress curl only (Figure 9b).

During the International Southern Ocean Studies (ISOS) several estimates from yearlong observation in 1975 on the Antarctic Circumpolar Current (ACC) volume transport through the Drake Passage were obtained: 110-138 Sv (1 Sv = 10^{6} m^3/s) (Nowlin et al., 1977), 139 ± 36 Sv (Bryden and Pillsbury, 1977), and 127 ± 14 Sv (Fandry and Pillsbury, 1977). Later, it was estimated as 118-146 Sv using a combination of moorings and hydrographic survey (Whitworth, 1983). Recently, this transport was estimated as 173.3 Sv (Donohue et al., 2016) with adding the near-bottom current meter measurements. It is not author 's intention to identify the basin-like mechanism (Stommel, 1957) or the channel-like mechanism (e.g., Johnson and Bryden, 1989) for the ACC's setup or to verify the accuracy of the Sverdrup and Stommel models using the observational data. However, these observations show the enhancement of the ACC volume transport through the Drake Passage (closer to the observational estimates) with the wind stress curl and JEBAG in comparison to that with the wind stress curl only.

8 Conclusions

Oceanographers take the vertical-deflected coordinate (λ, φ, z) [or (x, y, z)] instead of the vertical-true coordinate, and use the standard gravity $(-g_0)\mathbf{k}$ instead of the true gravity $\mathbf{g}$. In the vertical-deflected coordinate, the true gravity $\mathbf{g}$ has longitudinal-latitudinal component $\mathbf{g}_h$, which is neglected completely. This study demonstrates the importance of $\mathbf{g}_h$ in ocean circulation such as the geostrophic current, thermal wind, and wind-driven circulation in the (λ, φ, z) [or (x, y, z)] coordinate.

This additional force ($\mathbf{g}_h$) is added to the traditional geostrophic equation. Along with the traditional hydrostatic balanced equation, a new thermal wind equation is derived. The effect of $\mathbf{g}_h$ is evaluated using the two independent datasets: WOA18 for water density (ρ), and EIGEN-6C4 for the geoid (N). Non-dimensional C-number and D-number are proposed to identify relative importance of $\mathbf{g}_h$. The D-number (representing the relative importance of $\mathbf{g}_h$ versus deflected-horizontal density gradient on the thermal wind) increases with depth almost monotonically from a small value (0.084) at the surface ($z = 0$), and to 1.576 at $z = -5{,}000$ m. The horizontal gravity is an important force in ocean geostrophic motion.

Importance of $\mathbf{g}_h$ in the wind-driven ocean circulation is demonstrated using the combined Svedrup-Stommel-Munk equation with replacement of the standard gravity $(-g_0\mathbf{k})$ by the true gravity $\mathbf{g}$. An additional forcing (JEBAG) appears with comparable magnitude to the wind stress curl after being calculated from three independent datasets: SMD94 for wind stress ($\boldsymbol{\tau}$), WOA18 for water density (ρ), and EIGEN-6C4 for the geoid (N). The relative difference in the volume transport (with using the true gravity as the reference) is evident between standard and true gravities such as 0.373 in the Sverdrup volume transport streamfunction and 0.405 in the Stommel volume transport streamfunction. Observational data on the ACC volume transport through the Drake Passage show the importance of JEBAG in wind-driven ocean circulation.

Finally, if the oceanographic community wants to keep the traditional terminology about the vertical (normal to the Earth sphere/ellipsoid, i.e., the direction of $\mathbf{k}$) and the horizontal (Earth spherical/ellipsoidal surface, or x-y plane perpendicular to $\mathbf{k}$ in the local coordinate), the direction along the true gravity vector $\mathbf{g}$ ($= \mathbf{i}g_\lambda + \mathbf{j}g_\varphi + \mathbf{k}g_z$) should be called the **true vertical**; and the equipotential surfaces such as the geoid should be called the **true horizontal**.

Appendix A. Ellipsoidal Versus Spherical Coordinates

The ellipsoidal (or called oblate spheroid) coordinates share the same longitude (λ) but different latitude (φ_{ob}) and radial coordinate (representing vertical) (r_{ob}) with corresponding unit vectors ($\mathbf{i}$, $\mathbf{j}$, $\mathbf{k}$). The relationship between the oblate spheroid coordinates (λ, φ_{ob}, r_{ob}) and the polar spherical coordinates (λ, φ, r) is given by (Gill, 1982)

$$r^2 = r_{ob}^2 + \frac{1}{2}d^2 - d^2 \sin^2 \varphi_{ob}, \quad r^2 \cos^2 \varphi = (r_{ob}^2 + \frac{1}{2}d^2) \cos^2 \varphi_{ob} \qquad \text{(A1)}$$

where d is the half distance between the two foci of the ellipsoid. For the normal Earth, $d = 521.854$ km. The 3D vector differential operator in the oblate spheroid coordinates is represented by

$$\nabla_3 = \mathbf{i}\frac{1}{h_\lambda^{ob}}\frac{\partial}{\partial\lambda} + \mathbf{j}\frac{1}{h_\varphi^{ob}}\frac{\partial}{\partial\varphi} + \mathbf{k}\frac{1}{h_r^{ob}}\frac{\partial}{\partial z}, \qquad z = r - R \tag{A2}$$

where R = 6.3781364×10^6 m, is the semi-major axis of the normal Earth (Earth radius). The coefficients (or called Lame numbers) (h_λ^{ob}, h_φ^{ob}, h_r^{ob}) are given by

$$h_\lambda^{ob} = \sqrt{r^2 + \frac{1}{2}d^2}\cos\varphi,\ \ h_\varphi^{ob} = \sqrt{r^2 - \frac{1}{2}d^2 + d^2\sin^2\varphi},\ \ h_r^{ob} = \frac{r\sqrt{r^2 - \frac{1}{2}d^2 + d^2\sin^2\varphi}}{\sqrt{r^4 - \frac{1}{4}d^4}}. \tag{A3}$$

However, the 3D vector differential operator in the polar spherical coordinates is represented by

$$\nabla_3 = \mathbf{i}\frac{1}{R\cos\varphi}\frac{\partial}{\partial\lambda} + \mathbf{j}\frac{1}{R}\frac{\partial}{\partial\varphi} + \mathbf{k}\frac{\partial}{\partial z}. \tag{A4}$$

The difference between the two coordinates is 0.17% (Gill, 1982).

Appendix B. True Gravity and Its Approximation

The true gravity $\mathbf{g}$ is represented by a three-dimensional vector in the (λ, φ, z) coordinate system,

$$\mathbf{g} = \mathbf{g}_h + \mathbf{k}g_z,\ \ \mathbf{g}_h = \mathbf{i}g_\lambda + \mathbf{j}g_\varphi \tag{B1}$$

where $\mathbf{g}_h$ is the deflected-horizontal component, and $g_z\mathbf{k}$ the deflected-vertical component. It has two approximated forms. The first one is the normal gravity [$-g(\varphi)\mathbf{k}$] and usually represented in the oblate spheroid coordinates (see Appendix A) and associated with a mathematically modeled Earth (i.e., a rigid and geocentric ellipsoid) called the normal Earth. The normal Earth is a spheroid (i.e., an ellipsoid of revolution), has the same total mass and angular velocity as the Earth, and coincides its minor axis with the mean rotation of the Earth (Vaniček & Krakiwsky, 1986). The normal gravity vector [$-g(\varphi)\mathbf{k}$] is the sum of the gravitational and centrifugal accelerations exerted on the water particle by the normal Earth. Its intensity $g(\varphi)$ is determined analytically. For example, the World Geodetic System 1984 uses the Somiglina equation (National Geospatial-Intelligence Agency, 1984) to represent $g(\varphi)$

$$g(\varphi) = g_e\left[\frac{1+\kappa\sin^2\varphi}{\sqrt{1-e^2\sin^2\varphi}}\right],\ e^2 = \frac{a^2-b^2}{a^2},\ \ \kappa = \frac{bg_p - ag_e}{ag_e} \tag{B2}$$

where (a, b) are the equatorial and polar semi-axes; a is used for the Earth radius, $R = a$ = 6.3781364×10^6 m; b = 6.3567523×10^6 m; e is the spheroid's eccentricity; g_e = 9.780 m/s^2, is the gravity at the equator; and g_p = 9.832 m/s^2 is the gravity at the poles. The second one is the standard gravity vector, $-g_0\mathbf{k}$, with g_0 = 9.81 m/s^2. Oceanographer uses the standard gravity. Both normal and standard gravities don't have longitudinal-latitudinal component $\mathbf{g}_h$.

Appendix C. True, Normal, and Standard Gravity Potentials

Let (V, E, E_0) be the gravity potentials associated with the true gravity $\mathbf{g}$, the normal gravity $-g(\varphi)\mathbf{k}$, and the standard gravity $-g_0\mathbf{k}$. The potentials of the normal and standard gravities are given by

$$E(\varphi, z) = -g(\varphi)z, \quad E_0(z) = -g_0 z \tag{C1}$$

Both V and E include the potential of the Earth's rotation (P_R)

$$P_R = \Omega^2 r^2 \cos^2 \varphi / 2 \,). \tag{C2}$$

The gravity disturbance is the difference between the true gravity $\mathbf{g}(\lambda, \varphi, z)$ and the normal gravity $[-g(\varphi)\mathbf{k}]$ at the same point (Hackney & Featherstone 2003). The potential of the gravity disturbance (called the disturbing gravity potential) is given by

$$T = V - E = V + g(\varphi)z \tag{C3}$$

With the disturbing gravity potential T, the true gravity $\mathbf{g}$ ($= \mathbf{g}_h + g_z\mathbf{k}$) and its components are represented by (Sandwell & Smith, 1997)

$$\mathbf{g} = \nabla_3 V, \;\; \mathbf{g}_h = \nabla T, \;\; g_z = -g(\varphi) + \frac{\partial T}{\partial z} \tag{C4}$$

where $\nabla \equiv \mathbf{i}\frac{1}{R\cos\varphi}\frac{\partial}{\partial\lambda} + \mathbf{j}\frac{1}{R}\frac{\partial}{\partial\varphi}$ is the 2D vector differential operator. The geoid height (N) relative to the normal Earth (i.e., reference spheroid) is given by Bruns' formula (Chu 2018),

$$N(\lambda, \varphi) = \frac{T(\lambda, \varphi, 0)}{g_0} \tag{C5}$$

Eqs.(C3)-(C5) clearly show that the fluctuation of the marine geoid is independent of the Earth rotation and dependent on the disturbing gravity potential (T) evaluated at z = 0. The disturbing static gravity potential (T) outside the Earth masses in the spherical coordinates with the spherical expansion is given by (Kostelecký et al. 2015)

$$T(r, \lambda, \varphi) = \frac{GM}{r}\sum_{l=2}^{\infty}\sum_{m=0}^{l}\left(\frac{R}{r}\right)^{l}\left[\left(C_{l,m} - C_{l,m}^{el}\right)\cos m\lambda + S_{l,m}\sin m\lambda\right]P_{l,m}(\sin\varphi)\,, \tag{C6}$$

where $G = 6.674 \times 10^{-11}\mathrm{m^3kg^{-1}s^{-2}}$, is the gravitational constant; $M = 5.9736 \times 10^{24}$ kg, is the mass of the Earth; r is the radial distance with $z = r - R$; $P_{l,m}(\sin\varphi)$ are the Legendre associated functions with (l, m) the degree and order of the harmonic expansion; ($C_{l,m}, C_{l,m}^{el}, S_{l,m}$) are the harmonic geopotential coefficients (Stokes parameters with $C_{l,m}^{el}$ belonging to the reference ellipsoid. From Eqs. (C1) and (C3) the potential of the true gravity is given by

$$V = T - g(\varphi)z\,. \tag{C7}$$

From Eq.(C4) the true gravity is represented by

$$\mathbf{g}(\lambda, \varphi, z) = \nabla T + \left[\frac{\partial T}{\partial z} - g(\varphi)\right]\mathbf{k} \tag{C8}$$

The longitudinal-latitudinal component of the true gravity $\mathbf{g}_h$ at the reference spherical/ellipsoid surface (z = 0) is obtained using Eq.(C5) and Eq.(C8)

$$\mathbf{g}_h(\lambda, \varphi, 0) = \nabla T(\lambda, \varphi, 0) = g_0 \nabla N \tag{C9}$$

Appendix D. An Approximate 3D True Gravity Field for the Oceans

According to Eq.(C6) (i.e., the spectral of the disturbing static gravity potential T), the ratio between $T(\lambda, \varphi, z)$ to $T(\lambda, \varphi, 0)$ through the water column can be roughly estimated by

$$\left|\frac{T(\lambda, \varphi, z)}{T(\lambda, \varphi, 0)}\right| \approx \frac{R}{(R+z)} \approx 1, \qquad 0 \geq z \geq -H(\lambda, \varphi) \tag{D1}$$

where H is the water depth. Since R is the radius of the Earth and more than 3 orders of magnitude larger than H. This leads to the first approximation that the disturbing gravity potential $T(\lambda, \varphi, z)$ does not change with z in the whole water column (approximation of thin layer for the oceans)

$$T(\lambda,\varphi,z) \approx T(\lambda,\varphi,0), \quad 0 \ge z \ge -H(\lambda,\varphi) \tag{D2}$$

which makes

$$\nabla^2 T(\lambda,\varphi,z) \approx \nabla^2 T(\lambda,\varphi,0) \tag{D3}$$

Since the deviation of the vertical component of the gravity (g_z) to a constant ($-g_0$) is around 4 orders of magnitude smaller than g_0, it leads to the second approximation

$$g_z \approx -g_0 \tag{D4}$$

With the two approximations, the true gravity $\mathbf{g}$ in the water column is given by

$$\mathbf{g}(\lambda,\varphi,z) \approx \mathbf{g}(\lambda,\varphi,0) = g_0 \nabla N(\lambda,\varphi) - g_0 \mathbf{k} \tag{D5}$$

Where (C9) and (D2) are used. Correspondingly, the potential of the true gravity is approximately given by

$$V(\lambda,\varphi,z) \approx g_0 \left[N(\lambda,\varphi) - z \right] \tag{D6}$$

where Eq.(D5) is used.

Appendix E. Combined Sverdrup-Stommel-Munk Equation

Substitution of (4) and (5) into (15) gives the component form

$$-f\rho_0 v = -\frac{\partial p}{\partial x} + \rho g_0 \frac{\partial N}{\partial x} + \rho_0 K \frac{\partial^2 u}{\partial z^2} + \rho_0 A \nabla^2 u \,, \tag{E1}$$

$$f\rho_0 u = -\frac{\partial p}{\partial y} + \rho g_0 \frac{\partial N}{\partial y} + \rho_0 K \frac{\partial^2 v}{\partial z^2} + \rho_0 A \nabla^2 v \,, \tag{E2}$$

The Sverdrup-Stommel-Munk theories assume rigid lid surface (z = 0) and flat bottom (z = $-H$),

$$w|_0 = 0, \quad w|_{-H} = 0 \tag{E3}$$

and the wind stress (τ_x, τ_y) as the forcing at the ocean surface

$$\rho_0 K\left(\frac{\partial u}{\partial z}, \frac{\partial v}{\partial z}\right)\Big|_{z=0} = (\tau_x, \tau_y) \,. \tag{E4}$$

The bottom stress $(\tau_x^{(b)}, \tau_y^{(b)})$ was neglected (Sverdrup, 1947; Munk, 1950), or taken as the Rayleigh friction (Stommel, 1948),

$$\rho_0 K\left(\frac{\partial u}{\partial z}, \frac{\partial v}{\partial z}\right)\Big|_{z=-H} = (\tau_x^{(b)}, \tau_y^{(b)}) = \gamma \rho_0 (M_x, M_y), \tag{E5}$$

where

$$M_x = \int_{-H}^{0} u dz, \quad M_y = \int_{-H}^{0} v dz \tag{E6}$$

are the longitudinal and latitudinal volume transports per unit length, and γ is the Rayleigh friction coefficient.

Integration of the continuity equation (3b) with respect to z and use of the boundary conditions (E3) leads to

$$\frac{\partial M_x}{\partial x} + \frac{\partial M_y}{\partial y} = 0 \tag{E7}$$

Here, the volume transport stream function (Ψ) can be defined by

$$M_x = -\frac{\partial \Psi}{\partial y}, \quad M_y = \frac{\partial \Psi}{\partial x} \tag{E8}$$

Integration of the momentum equations (E1) and (E2) with respect to z from $z = -H$ to $z = 0$ and use of (E4) and (E5) lead to

$$-A\nabla^2 M_x - fM_y = -\frac{1}{\rho_0}\int_{-H}^{0}\frac{\partial p}{\partial x}dz + g_0\int_{-H}^{0}\frac{\rho}{\rho_0}\frac{\partial N}{\partial x}dz + \frac{\tau_x - \tau_x^{(b)}}{\rho_0} \tag{E9}$$

$$-A\nabla^2 M_y + fM_x = -\frac{1}{\rho_0}\int_{-H}^{0}\frac{\partial p}{\partial y}dz + g_0\int_{-H}^{0}\frac{\rho}{\rho_0}\frac{\partial N}{\partial y}dz + \frac{\tau_y - \tau_y^{(b)}}{\rho_0} \tag{E10}$$

Cross differentiation of (E9) and (E10) with respect to x and y leads to the combined Sverdrup-Stommel-Munk equation with $\mathbf{g}_h$,

$$-A\nabla^4\Psi + \gamma\nabla^2\Psi + \beta\frac{\partial \Psi}{\partial x} = \frac{1}{\rho_0}\left[\mathrm{curl}\,\boldsymbol{\tau} + g_0\int_{-H}^{0} J(\rho, N)dz\right] \tag{E11}$$

where $\beta = (2\Omega\cos\varphi)/R$; and $J(\rho, N) \equiv (\partial\rho/\partial x)(\partial N/\partial y) - (\partial\rho/\partial y)(\partial N/\partial x)$, is the Jacobian of ρ and N. Without $\mathbf{g}_h$ (i.e., $\nabla N = 0$), Eq.(E11) is reduced to Eq.(5.5.29) in the reference (Pedlosky, 1984).

Acknowledgements

The author thanks Mr. Chenwu Fan's outstanding efforts on computational assistance, and the International Centre for Global Erath Models (ICGEM) for the geoid [$N(\lambda, \varphi)$] data of the EIGEN-6C4 model (http://icgem.gfz-potsdam.de/home), the NOAA National Centers for Environmental Information (NCEI) for the WOA18 annual mean hydrographic data (https://www.nodc.noaa.gov/OC5/woa18/), the International Research Institute for Climate and Society for the SMD94 annual mean wind stress $(\tau_\lambda, \tau_\varphi)$ data (http://iridl.ldeo.columbia.edu/SOURCES/.DASILVA/.SMD94/.climatology/), and the NASA Jet Propulsion Laboratory for the OSCAR third degree resolution 5-day mean surface current vectors $\mathbf{U}(\lambda, \varphi)$ data (https://podaac-tools.jpl.nasa.gov/drive/files/allData/oscar/).

References

Bryden, H. L., & Pillsbury, R. D. (1977). Variability of deep flow in the Drake Passage from year-long current measurements. *Journal of Physical Oceanography*, *7*, 803-810.

Chu, P.C. (2018). Two types of absolute dynamic ocean topography. *Ocean Science*, *14*, 947-957, https://doi.org/10.5194/os-14-947-2018.

Chu, P.C. (2021). Ocean dynamic equations with the real gravity. *Nature Scientific Reports*, *11*, Article Number 3235.

da Silva, A. Young, A. C., & Levitus, S. (1994). *Atlas of Surface Marine Data 1994*, Volume 1: Algorithms and Procedures, Number 6.

Donohue, K. A., Tracey, K. L., Watts, D. R., Chidichimo, M. P., & Chereskin, T. K. (2016). Mean Antarctic Circumpolar Current transport measured in Drake Passage, *Geophysica. Research Letters*, *43*, 11,760–11,767, doi:10.1002/2016GL070319.

Fandry, C., & Pillsubury, R. D. (1979). On the estimation of absolute geostrophic volume transport applied to the Antarctic Circumpolar Current. *Journal of Physical Oceanography*, *9*, 449-455.

Förste, C., Bruinsma, S.L., Abrikosov, O., Lemoine, J.M., Marty, J.C., Flechtner, F., Balmino, G., Barthelmes, F., & Biancale, R. (2014). EIGEN-6C4. The latest combined global gravity field model including GOCE data up to degree and order 2190 of GFZ Potsdam and GRGS Toulouse, http://doi.org/10.5880/icgem.2015.1.

Gill, A.E. (1982). *Atmosphere-ocean dynamics*. *International geophysics series* (Vol 30), Academic Press, New York, 91-94.

Hackney, R.I., & Featherstone, W.E. (2003). Geodetic versus geophysical perspectives of the 'gravity anomaly'. *Geophysical Journal International*, *154*, 35-43.

Ince, E.S., Barthelmes, F., Reiβland, S., Elger, K., Förste, C., Flechtner, F., & Schuh, H. (2019). ICGEM – 15 years of successful collection and distribution of global gravitational models, associated services, and future plans. *Earth System Scientific Data*, *11*, 647 -674.

Johnson, G.C., & Bryden, H. (1989). On the strength of the circumpolar current. *Deep Sea Research*, *36*, 39-53.

Kostelecký, J., Klokočnik, J., Bucha, B., Bezděk, A., & Förste, C. (2015). Evaluation of the gravity model EIGEN-6C4 in comparison with EGM2008 by means of various functions of the gravity potential and by BNSS/levelling. *Geoinformatics FCE CTU*, *14 (1)*, http://doi.org//10.14311/gi.14.1.1.

Munk, W.H. (1950). On the wind-driven ocean circulation. *Journal of Meteorology*, *7*, 79-93.

National Geospatial-Intelligence Agency (1984). *Department of defense world geodetic system 1984 (WGS84)*. Its definition and relationships with local geodetic systems. NIMA TR8350.2., 3rd Edition, Equation 4-1.

Pedlosky, J. (1987). *Geophysical fluid dynamics* (Second Edition), Springer, New York, 200-212.

Sandwell, D.T., & Smith, W.H.F. (1997). Marine gravity anomaly from Geosat and ERS 1 satellite altimetry. *Journal of Geophysical Research, 102*, 10,039-10,054.

Stommel, H. (1948). The westward intensification of wind-driven ocean currents. *Transaction American Geophysical Union*, **29** (2), 202-206.

Stommel, H. (1957). A survey of ocean current theory. *Deep Sea Research*, *6*, 149-184.

Sverdrup, H. U. (1947). Wind-driver currents in a baroclinic ocean; with application to the equatorial current of the eastern Pacific, *Proceedings National Academy of Sciences*, *33*, 318-326.

Vaniček, P, & Krakiwsky, E. (1986). *Geodesy: the concepts*. Part 5 Earth gravity field, North-Holland, Amsterdam, 457-581.

Whitworth, T. (1983). Monitoring the transport of the Antarctic Circumpolar Current at Drake Passage. *Journal of Geophysical Research*, *13*, 2,045-2,057.

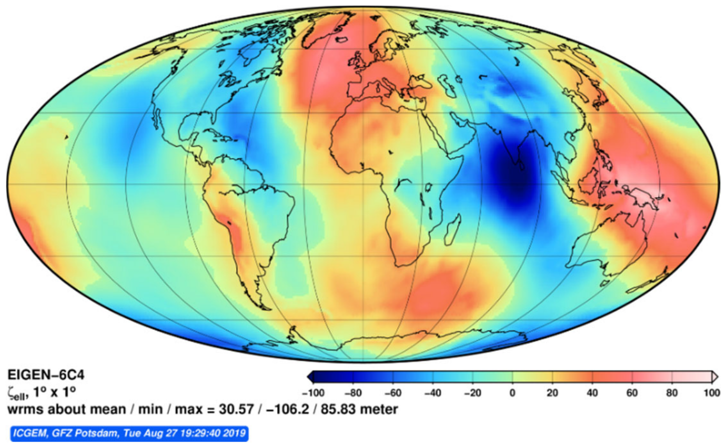

Figure 1. Digital data for EIGEN-6C4 geoid undulation (*N*) with 1º×1º, computed online at the website http://icgem.gfz-potsdam.de/home.

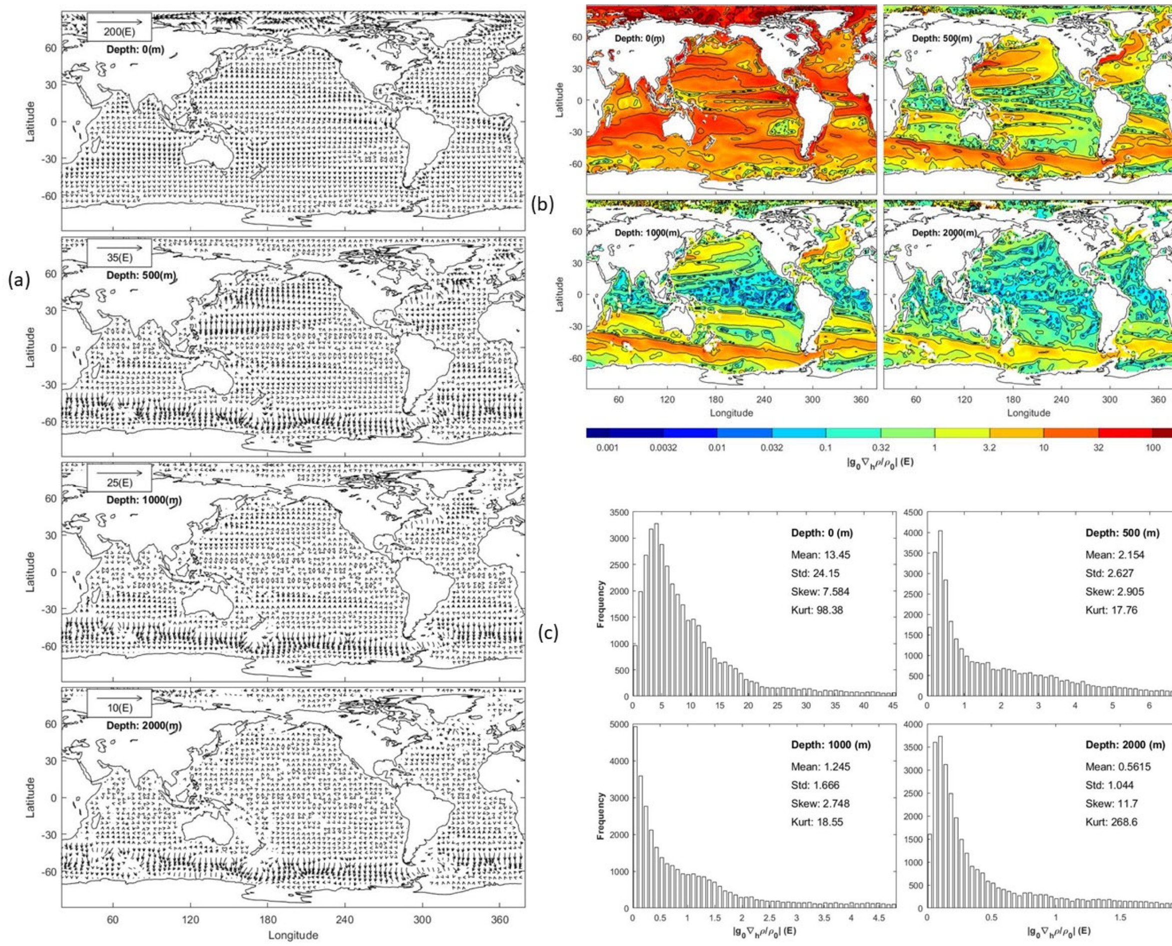

Figure 2. Horizontal density gradient $(g_0/\rho_0)\nabla\rho$ at the four levels (z = 0, -500 m, -1,000 m, and -2,000 m): (a) the vector plots, (b) contour plots of the magnitudes $|(g_0/\rho_0)\nabla\rho|$, and (c) histograms of $|(g_0/\rho_0)\nabla\rho|$. The magnitude $|(g_0/\rho_0)\nabla\rho|$ has the mean of 13.45 E (1E $=10^{-9}s^{-2}$) at the surface (z = 0), 2.154 E at z = -500 m, 1.245 E at z = -1,000 m, and 0.5615 E at z = - 2,000 m.

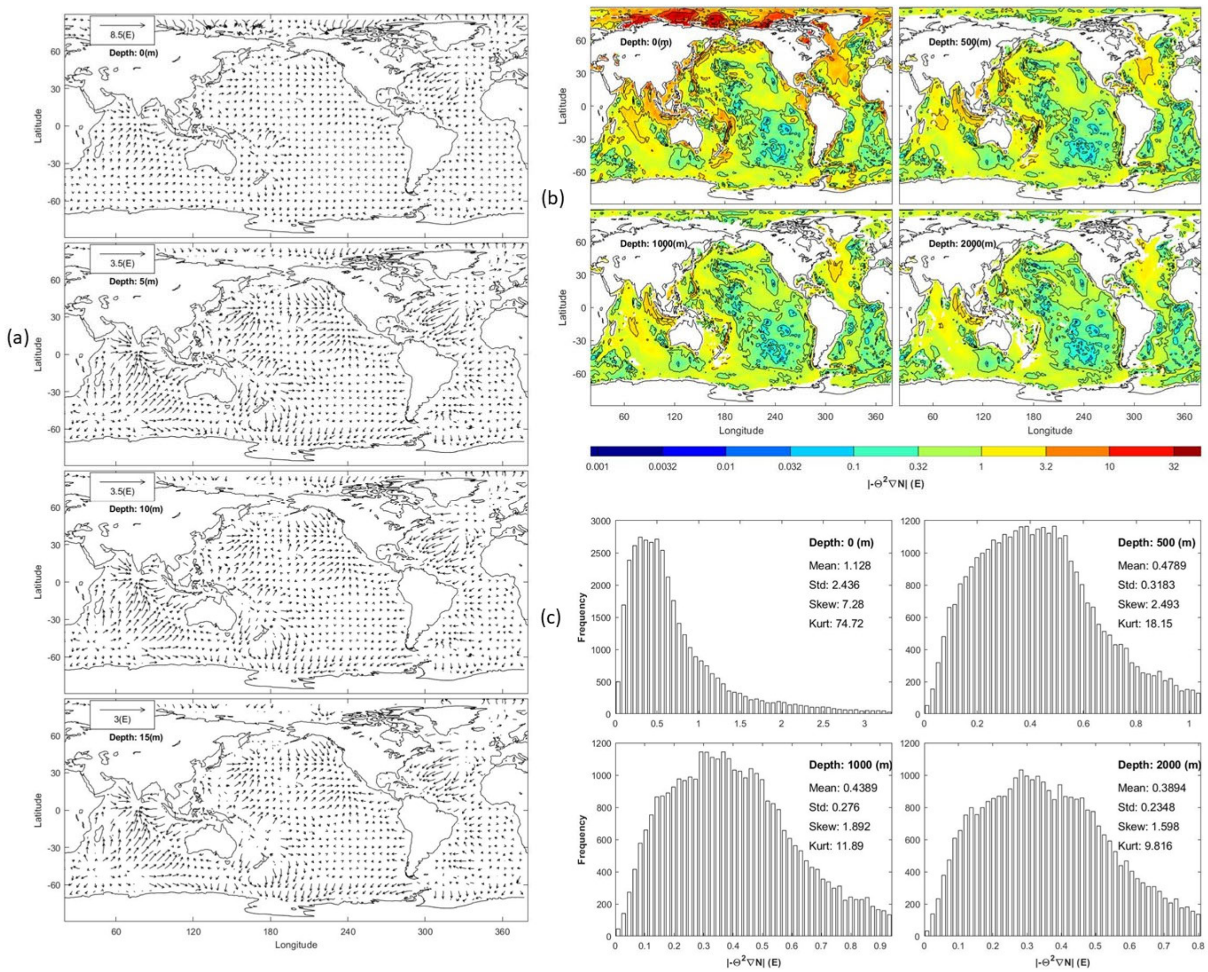

Figure 3. Horizontal gradient $-\Theta^2\nabla N$ at the four levels (z = 0, -500 m, -1,000 m, and -2,000 m): (a) the vector plots, (b) contour plots of the magnitudes $|-\Theta^2\nabla N|$, and (c) histograms of $|-\Theta^2\nabla N|$. The magnitude of $|\Theta^2\nabla N|$ has the mean of 1.128 Eotvos (E) at the surface (z = 0), 0.4789 Eotvos (E) at z = -500 m, 0.4389 Eotvos (E) at z = -1,000 m, and 0.3894 Eotvos (E) at z = -2,000 m.

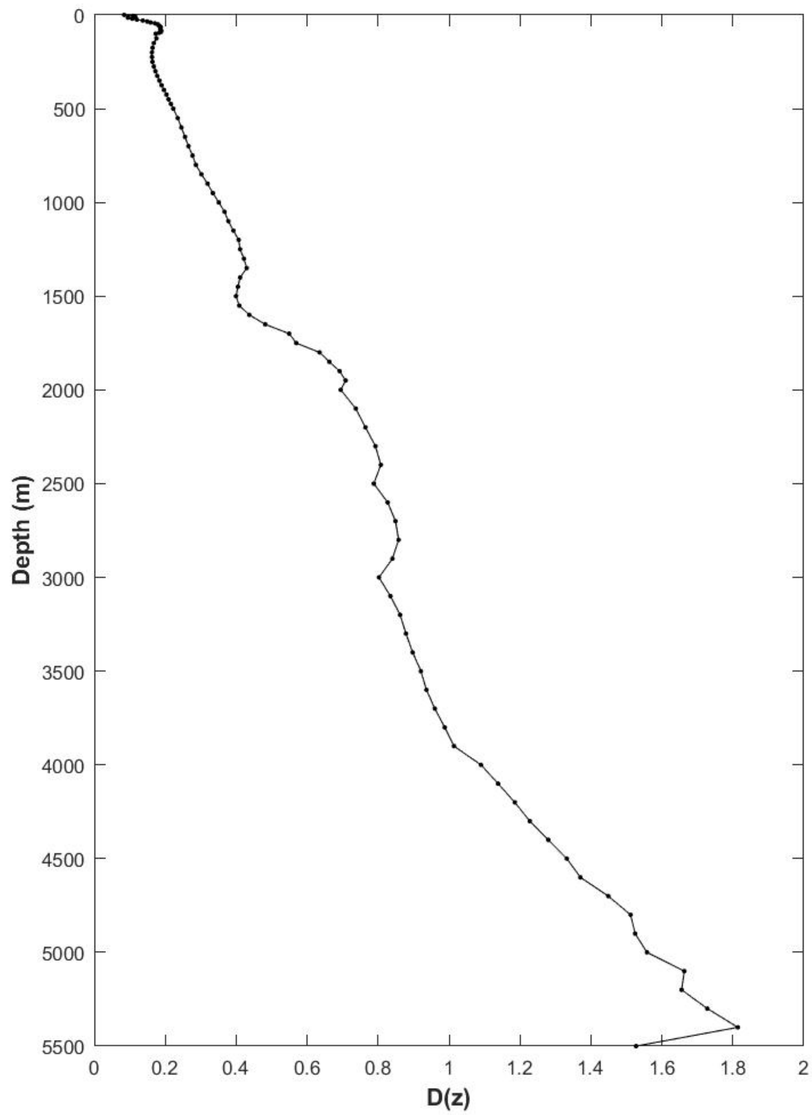

Figure 4. Depth dependent D-number calculated from the EIGEN-6C4 and WOA18 Datasets.

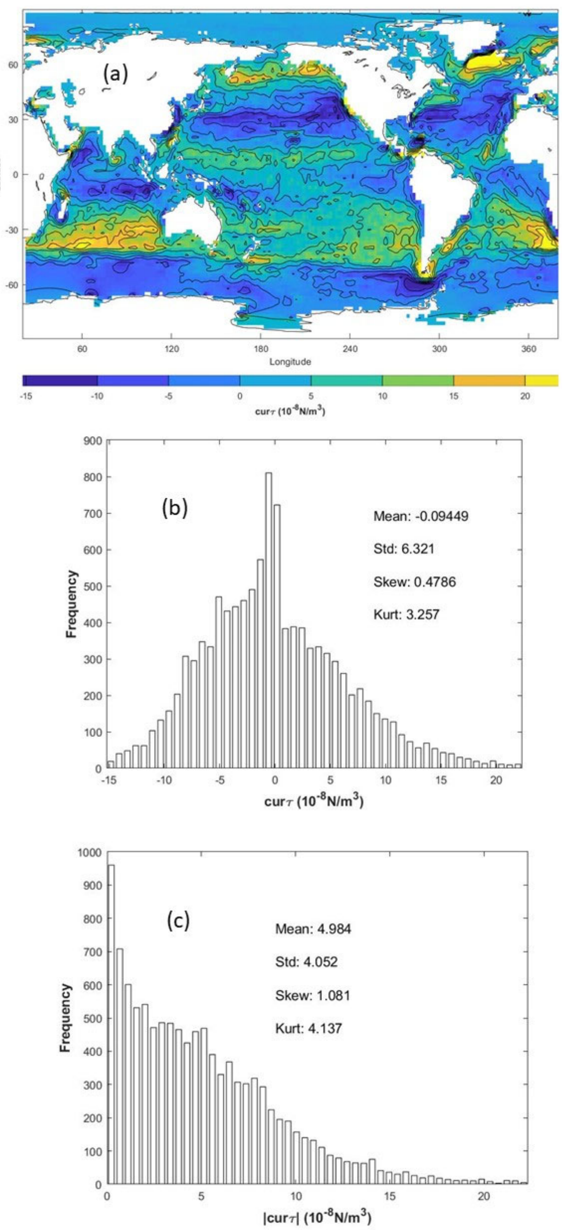

Figure 5. Climatological annual mean surface wind stress curl (unit: 10^{-8} Nm^{-3}) calculated using the COADS data: (a) contour plot of $(\text{curl}\ \boldsymbol{\tau})$, (b) histogram of $(\text{curl}\ \boldsymbol{\tau})$, (c) histogram of $|\text{curl}\ \boldsymbol{\tau}|$.

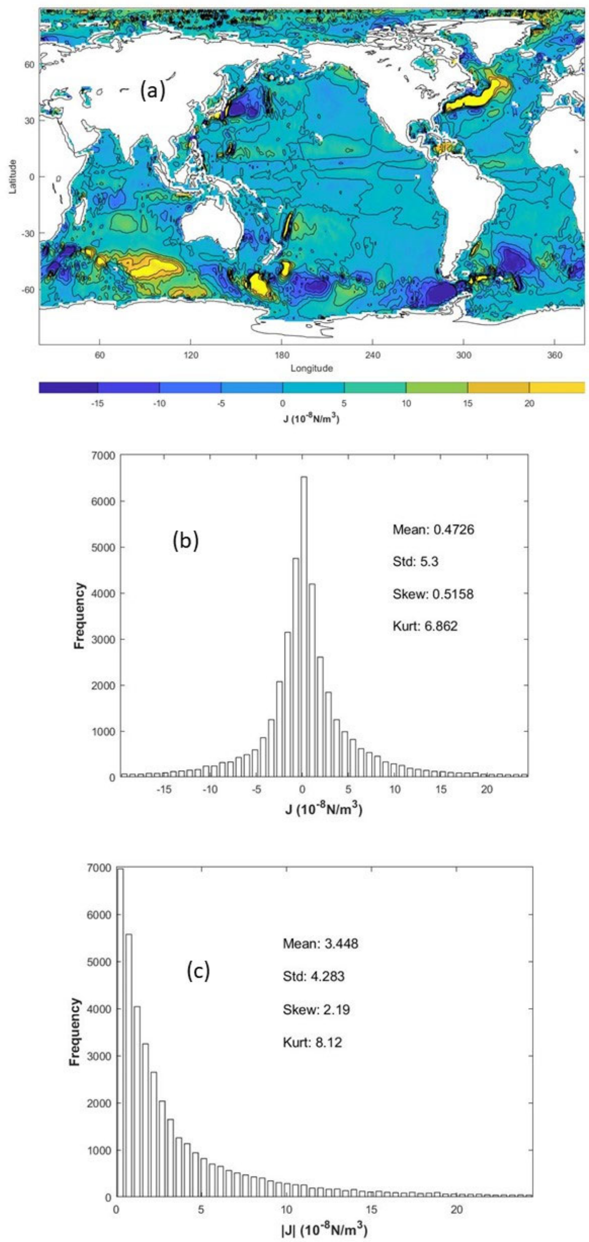

Figure 6. Climatological annual mean JEBAG (unit: 10^{-8} Nm^{-3}) calculated using the NOAA/NCEI WOA18 annual mean temperature and salinity data and the EIGEN-6C4 geoid undulation (*N*) data: (a) contour plot of JEBAG, (b) histogram of JEBAG, and (c) histogram of |JEBAG|. Note that JEBAG is simplified by 'J' here.

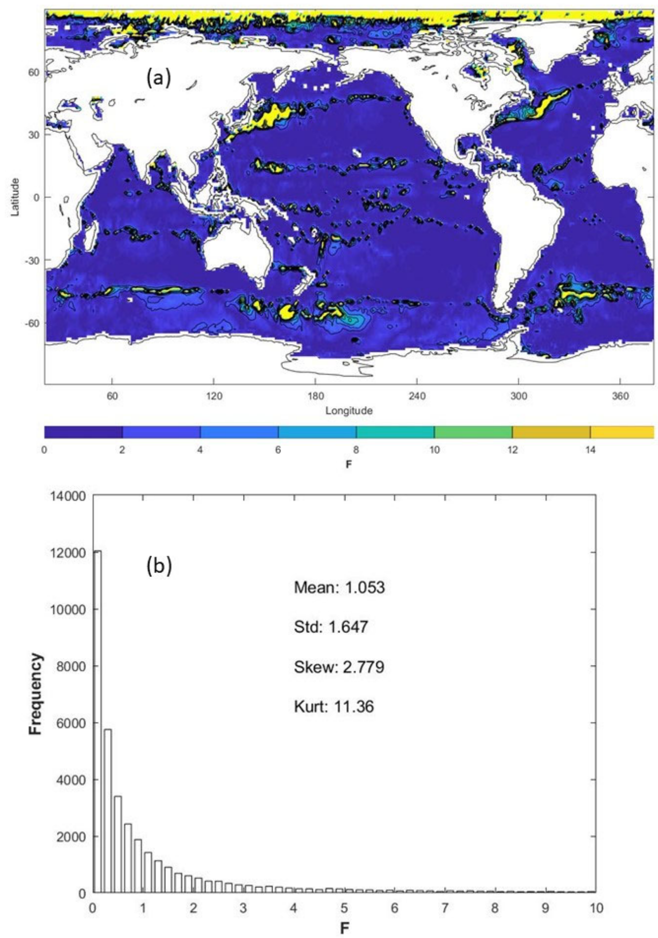

Figure 7. Climatological annual mean F number calculated using the WOA18 hydrographic data, the COADS surface wind stress curl, and the EIGEN-6C4 geoid height (N) data: (a) contour plot of $F(\lambda, \varphi)$, and (b) histogram of F.

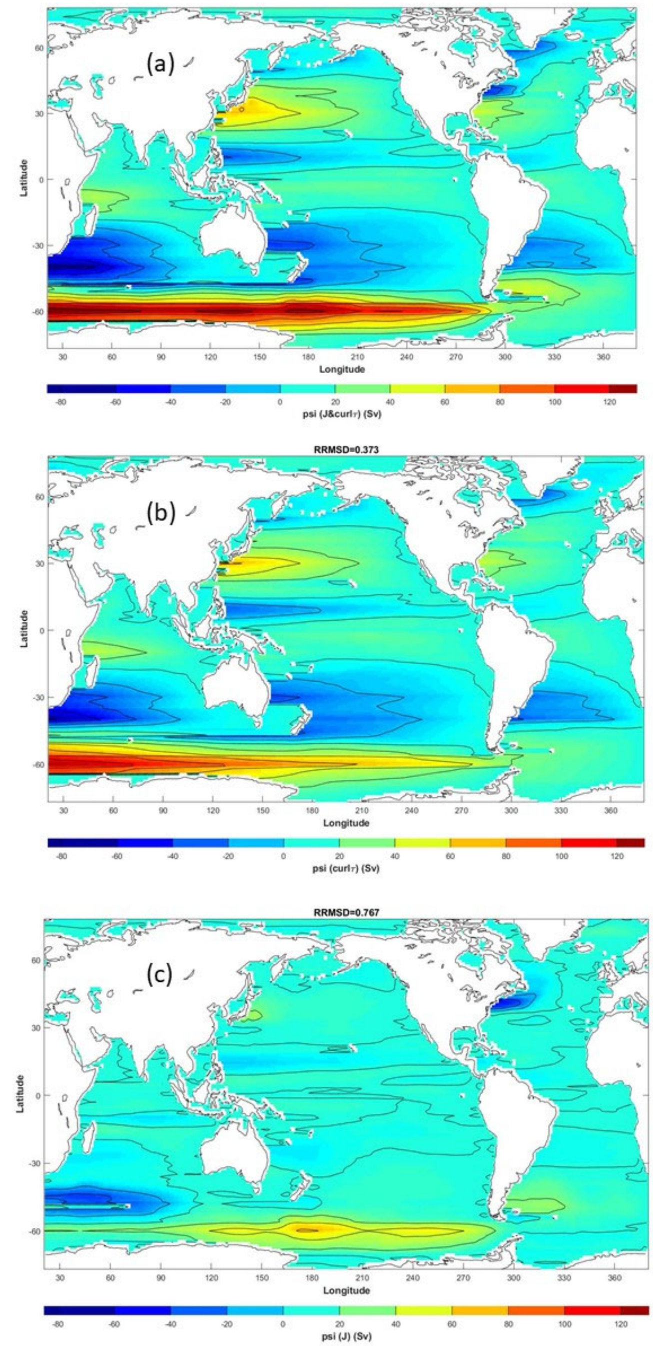

Figure 8. Sverdrup volume transport streamfunction (unit: Sv) with (a) wind stress curl and JEBAG, (b) wind stress curl, (c) JEBAG.

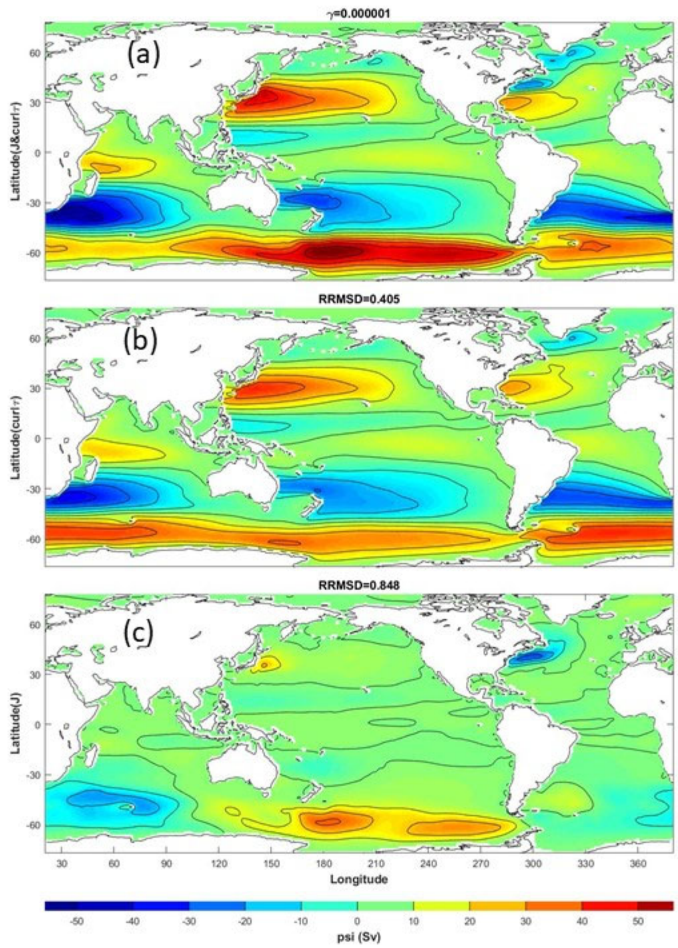

Figure 9. Stommel volume transport streamfunction (unit: Sv) with (a) wind stress curl and JEBAG, (b) wind stress curl, and (c) JEBAG.